# Orbit determination of the Near-Earth asteroid 1985 JA

Team 8: United eggs

[a]*Anna James, José María Salvador, Nurkyz Ydyrysova*

**Abstract**

This report presents the results of a study on the orbit of the near-Earth asteroid 1985 JA. Using astrometry, we closely observed the asteroid over several weeks to accurately calculate its orbital coordinates. Using the Method of Gauss, we determined the six orbital elements of the asteroid, characterizing its orbit. The calculated orbital elements are as follows: semi-major axis (a) = 1.65 AU, eccentricity (e) = 0.32, inclination (i) = 36.8°, the longitude of ascension ($\Omega$) = 232.5°, argument of periapsis ($\omega$) = 288.9°, and mean anomaly (M) = 70°. The accuracy of the orbital elements was confirmed through comparisons with values obtained from the JPL Horizons' Website [6]. The percent differences for these orbital elements were mostly 1 percent. We also reconstructed the asteroid's right ascension (RA) and declination (dec) from the position and velocity vectors, achieving excellent accuracy, with percent differences well below 1 percent. Factors such as adverse climatic conditions and the asteroid's low apparent magnitude presented certain challenges in our analysis. To better future research, we recommend selecting a period when the asteroid has a lower apparent magnitude and seeking observation locations with better climatological conditions. Additionally, extending the study to incorporate more observations and considering long-term orbital predictions and spin-related variations would provide valuable insights. Our research demonstrates the feasibility of orbit determination for near-Earth asteroids using a limited number of observations and highlights the potential for further investigations in this field.

## 1. Introduction

### *1.1. Space Debris*

There are many pieces of space debris in our unique Solar System. These "space scraps" originate from the creation of our current solar system [15]. Some examples of these "space scraps" are comets and asteroids.

Comets are icy pieces of rock, gases, and dust [3] that lighten as they approach the Sun and leave a tail that lengthens as the comet gets closer to the Sun [12]. They also have unique, elongated orbits that aren't restricted by the plane of the planets' and asteroids' orbits, which depend on the location of the comets. Two places comets are found are the Kuiper Belt, which is between Neptune and Pluto, and the Oort Cloud, which is a spherical cloud that surrounds the Solar System [14].

The other type of space debris is asteroids. Asteroids are small pieces of rock that orbit the Sun[11]. Most of these asteroids orbit around Mars and Jupiter. However, some asteroids are

located in the Kuiper Belt. Similar to comets, asteroids have unique orbits that aren't circular. An example of an asteroid is Ceres, which is the largest type of asteroid. There are three types of asteroids: C-type, S-type, and M-type. C-type asteroids are the most common and are made of mostly carbon. S-type asteroids are mostly made of silicon. Lastly, M-type asteroids are made of nickel-iron.

### *1.2. Near-Earth Asteroids and Mars crossing asteroids*

Mars-crossing asteroids are asteroids that cross Mars' orbits [9]. Near-Earth asteroids are asteroids who travel close to the Earth's orbit [4]. These asteroids are mostly in the inner solar system between Jupiter and Mars and make up about a third of the asteroids in our solar system. More specifically, these asteroids are less than 1.3 astronomical units (AU) from the Sun. [2].

Currently, near-Earth asteroids are still being discovered today. The asteroids that have been found are categorized by their sizes. For instance, 90 percent of the large asteroids, which are asteroids that have a diameter over 1 kilometer, are known. In contrast, many of the smaller, but still hazardous, asteroids haven't been found. For example, about 1 percent of asteroids around the size of 40 meters to 140 meters have been found[7].

Since many of these dangerous asteroids haven't been found, there are multiple search campaigns dedicated to tracking them. For example, the Department of Defense uses a global Space Surveillance Network (SSN) to observe space junk, such as near-Earth Asteroids. Additionally, NASA funds a program called Double Asteroid Redirection Test or "DART", which monitors a binary asteroid system called Didymos [1]. "DART" is an organization whose purpose is to deflect the path of the binary system of asteroids. The reasoning behind this is to hopefully be able to use this same process to deflect any possible asteroid that could hit the Earth.

### *1.3. 1985 JA Asteroid*

The asteroid we chose to use is the 1985 JA or 3553 Mera Asteroid. 1985 JA's asteroid's orbit is described by six different characteristics or elements. First element to describe an asteroid's orbit is the semi-major axis, which gives the size of the elliptical orbit. The second element, eccentricity, describes the stretching or lengthening of the asteroid's orbit. Inclination, the third element, represents the angle between the field of the asteroid's orbit and the field of Earth's orbit. The fourth element is the longitude of the ascending node between the Spring Equinox and ascending node. The fifth characteristic that describes an asteroid's orbit is the argument of perihelion, which is the angle between the longitude of ascending node and its perihelion, which is the point of closest approach to the Sun. The last element of the asteroid's orbit is the mean anomaly, which is the angular position of a test body on a circular orbit with a radius equal to the semi-major axis.

To determine the orbit of our asteroid, 1985 JA, we used the Method of Gauss. This process involved iterating through data to determine the position and velocity vector of the asteroid with respect to the Sun. The data originated from three, equally spaced observations. From the position and velocity vectors, the orbital elements can get be calculated. Thus, the asteroid's orbit can be fully determined.

| **Date / Time (UT) of each observation session** | **June 17<br>5AM - 7AM** | **June 26<br>3AM - 5AM** | **June 30<br>3AM - 5AM** | **July 5<br>3AM - 5AM** |
|---|---|---|---|---|
| **Predicted position of our asteroid** | RA = 16:07:31.44<br>Dec = +19 19' 54" | RA = 16:01:01.92<br>Dec = +20 52' 10' | RA = 15:59:26.03<br>Dec = +21 11' 03" | RA = 15:58:25.30<br>Dec = +21 20' 19.9" |
| **Information about images** | Images taken: 9<br>Filter: Open<br>Exposure time:<br>60s (3 lights, 3 darks)<br>120s (4 lights, 4 darks)<br>600s (2 lights, 1 dark)<br>Biases: 10<br>Flats: 5 | Images taken: 10<br>Filter: Open<br>Exposure time:<br>120s (4 lights, 4 darks)<br>180s (5 lights, 4 darks)<br>600s (1 light)<br>Biases: 4<br>Flats: 4 | Images taken: 14<br>Filter: Open<br>Exposure time:<br>120s (5 lights, 5 darks)<br>180s (8 lights, 8 darks)<br>600s (1 light)<br>Biases: 5<br>Flats: 0 | Images taken: 6<br>Filter: Open<br>Exposure time:<br>180s (2 lights, 2 darks)<br>240s (1 light, 1 dark)<br>300s (3 lights, 3 darks)<br>Biases: 5<br>Flats: 0 |
| **Notes** | Relatively good quality, as the asteroid is visible in some of the longer exposure images.<br>(Asteroid found) | Bad quality mainly due to the weather, so the images were not particularly useful.<br>(Asteroid not found) | The sky was relatively clear, but there was some smoke, which partially affected the image quality.<br>(Asteroid not found) | There was some smoke due to fireworks, though the sky was still relatively clear.<br>(Asteroid found) |

Table 1: Table detailing our observations in chronological order.

## 2. Data Acquisition

### *2.1. Observations*

We observed 4 times at Morehead Observatory at the University of North Carolina in Chapel Hill, with two of them being successful. The observations were done using a 0.6m (24") professional Perkin-Elmer telescope. The telescope is equipped with several CCD cameras, including one attached to a stellar spectrometer[1]. Two software programs were used to process astronomical images. AstroImageJ (AIJ) handled dark subtraction, bias subtraction, and flat division to correct instrumental errors. It also aligned the images to track the asteroid's movement. DS9 was employed for astrometry and photometry, providing approximations of equatorial coordinates and apparent visual magnitude for each observation. In addition to the observations at the Morehead Observatory, one additional observation was conducted remotely at the Sierra Remote Observatory in Auberry, California, USA (MPC U69) through the "iTelescope" network. This observatory is equipped with a 0.61-m f/6.5 reflector telescope and a CCD. The Sierra Remote Observatory, situated in the surroundings of the Sierra Nevada Mountains, benefits from clear and sunny skies. Efficient and productive observation sessions were ensured through careful preparation. This involved obtaining printed ephemeris from JPL Horizons for accurate positional data of the asteroid. A star chart printed from DS9 was used to anticipate the asteroid's path, aiding in telescope positioning and locating the asteroid during and after the observation. We list our observations in Table 1. As shown in the table, we had 4 observations at Morehead observatory, from which only 2 were observable (Figure 1), and our last observation was taken remotely at the Sierra Remote Observatory. Overall, we have 9 good images from 3 observations.

[1]https://physics.unc.edu/research-pages/astronomy-and-astrophysics/unc-observatories/

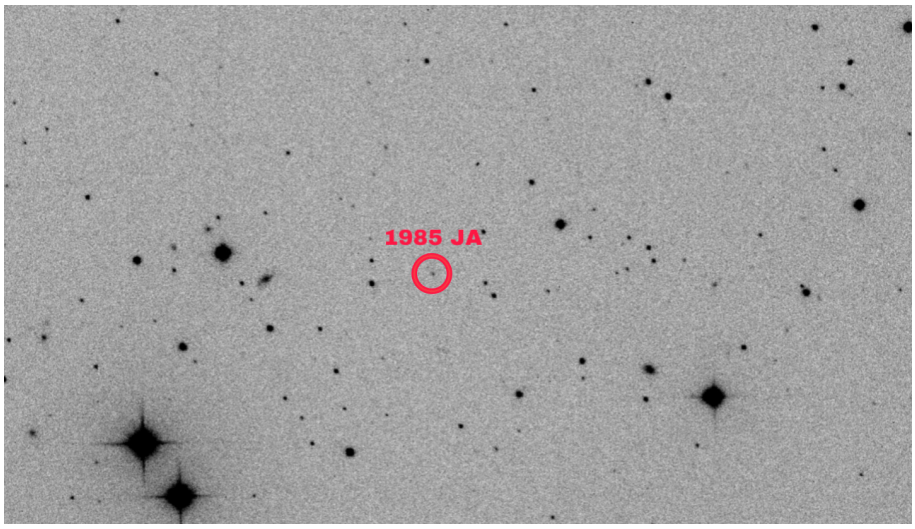


Figure 1: An image of our found asteroid.

### *2.2. Image Reduction with Astrometry*

The first step in obtaining accurate positional data from astronomical images is using astrometry. Astrometry involves transforming x and y coordinates into equatorial coordinates. Around ten reference stars with known coordinates were chosen from databases USNO UCAC5 using DS9 software to establish the relationship between equatorial and x and y coordinates. Then using DS9 we created regions and used the centroiding function to find the right ascension and declination of our asteroid.

### *2.3. Determination of Errors in Astrometry*

Once the RA and DEC were calculated through DS9 centroiding, the uncertainties for these coordinates were completed through astrometry.net website[2]. We calculated the uncertainties with this website by downloading a corr fits file, which gave a table of calibrated and expected locations for every object that was used by astrometry in the plate solution. This was used as a numpy array and the root of the mean of the square distances (RMS) was calculated through this file. Thus, the RMS was used to characterize the uncertainty of the RA and DEC.

The calculated positional coordinates for the asteroid had an uncertainty of less than 1 arcsecond. These results were subsequently employed to calculate the positional and velocity vectors of 1985 JA through the Method of Gauss and to identify deviations between the calculated fit coordinates and the observed coordinates.

[2]astrometry.net

| Date (UT) | RA (hh:mm:ss) | Uncertainty (s) | DEC (degrees, arcmin, arcsec) | Uncertainty (arcsec) |
|---|---|---|---|---|
| June 17, 2023 | 16:07:27.89 | ± 0.00011 | +19:20:45.39 | ± 0.000036 |
| July 5, 2023 | 15:58:25.19 | ± 0.000026 | +21:20:20.23 | ± 0.000065 |
| July 8, 2023 | 15:58:19.49 | ± 0.0000014 | +21:19:16.85 | ± 0.000016 |

### *2.4. Photometry*

Photometry, similar to astrometry, involves comparing data from an image and a database to find the instrumental and visual magnitude. The process of obtaining photometric data begins by calculating the relative brightness of stars within an image. Stars serve as known objects with documented apparent visual magnitudes. To calculate the visual magnitudes (Rmag) of the diffferent stars, the catalog USNO UCAC5 was used.

Then, aperture photometry is employed. This process computes an instrumental magnitude for a specified aperture and annulus within the image. The aperture represents a circular area of interest, while the annulus creates a ring of pixels surrounding the center, providing an average sky value around the object. Due to the square shape of pixels, accurately approximating a circle, especially for smaller regions of interest, can be challenging. To address this, the signal value of pixels is weighted based on the fraction of each pixel within the circle. This modified approach allows for the determination of the average signal of the pixels in the image.

The combined aperture and annulus are used to calculate the overall signal and the signal-to-noise ratio (SNR) of the region of interest. The signal (S) is computed by summing the pixel counts within the aperture and subtracting the average sky value. The SNR represents the ratio of the signal to the total uncertainty or noise (N) present in the image. Using the SNR and signal, an instrumental magnitude is calculated for the area within the aperture. This instrumental magnitude serves as a relative measure of brightness that can be compared with other parts of the same image. After calculating the instrumental magnitudes and collecting the apparent visual magnitudes of ten stars, a line of best fit is used to give a linear relationship between the two. The instrumental magnitude of the asteroid can then be calculated and graphed on the line, resulting in an approximate apparent visual magnitude. The uncertainty is then calculated using Formula 1.

$$\sigma = \frac{1.0875}{\text{SNR}} \tag{1}$$

| Obs | Date (UT) | RMag | Uncertainty |
|---|---|---|---|
| 1 | June 17, 2023 | 17.27 | ±0.65 |
| 2 | July 5, 2023 | 18.66 | ±0.43 |
| 3 | July 8, 2023 | 18.6 | ±0.71 |

Table 2: Table detailing observation time, along with the respective averaged 'r' magnitude from each set of observations

## 3. Additional information of Observations

In addition to the apparent magnitude and celestial coordinates, we present the Julian Date (JD) at which each observation session was undertaken. Furthermore, 3553 Mera has an approximate diameter somewhere between 1.369 and 3.062 kilometers, making it much larger than 99% of asteroids[3]. Finally, it has an absolute (H) magnitude of 16.43[4].

| Observation | JD | RA | Declination |
|---|---|---|---|
| **1** | 2460112.77 | 16:07:27.90 | 19°20' 45.39" |
| **2** | 2460130.70 | 15:58:25.01 | 21°20' 20.39" |
| **3** | 2460133.79 | 15:58:19.51 | 21°19' 16.82" |

Table 3: Detailing different aspects of our observations such as Julian Date (JD), right ascension (RA) and declination

## 4. Orbit Determination

### *4.1. Methods*

The positional data obtained through astrometry provides values for right ascension and declination. However, a crucial piece of information is missing: the distance of the asteroid from Earth.

To describe the positional relationship between the Earth, the Sun, and a specific celestial body, like our asteroid, three vectors are considered: $\vec{r}$, $\vec{R}$, and $\vec{p}$. The vector $\vec{r}$ represents the direction from the sun to the celestial body, $\vec{R}$ represents the direction from the Earth to the Sun, and $\vec{p}$ represents the direction from the Earth to the celestial body. Spherical trigonometry allows the determination of the direction of $\vec{p}$, denoted as $\hat{p}$ based on a given right ascension (RA) and declination (dec), as given by the following equation, where $\alpha$ is right ascension and $\beta$ is declination.

$\hat{p} = (\cos\alpha \cdot \cos\delta)\mathbf{i} + (\sin\alpha \cdot \cos\delta)\mathbf{j} + (\sin\delta)\mathbf{k}$

From simple vector manipulations, we obtain $\vec{r}$ and $\dot{\vec{r}}$ . Moreover, the orientation of the orbit in three-dimensional space can be determined by taking the cross product of $\vec{r}$ and $\dot{\vec{r}}$. Therefore, the angular momentum per unit mass can be found using Formula 2.

$$\vec{h} = (\vec{r} \times \dot{\vec{r}}) \tag{2}$$

[3]https://www.spacereference.org/asteroid/3553-mera-1985-ja

[4]https://ssd.jpl.nasa.gov/horizons/app.html/

*4.1.1. The Method of Gauss*

The Method of Gauss and the Method of Laplace are primary orbit determination methods that use observational data to calculate $\vec{r}$ and $\dot{\vec{r}}$. Unlike the Method of Laplace, the Method of Gauss uses Kepler's second law directly and is the best for small near-earth bodies like our asteroid, so in this research, we use the former one [8]. Three observations of a body must be made for the Method of Gauss, along with the corresponding right ascensions, declinations, and observation times. With these inputs, it is possible to determine the body's $\vec{r}$ and $\dot{\vec{r}}$ for each observation, where the subscripts 1, 2, and 3 denote the first, second, and third observations, respectively. In the Method of Gauss, the units of time must be changed from standard time into Gaussian time, centered on the middle observation. The unit of Gaussian time is the Gaussian day. To find the Gaussian time for our observation, we multiplied the difference of times by the Gaussian constant, $k$, approximately equal to 0.0172021 for the purposes of this system.

By considering the conservation of angular momentum, we determined that all three position vectors lie in the same plane. Thus, the central observation position vector, $\vec{r}_2$, can be expressed as a linear combination of $\vec{r}_1$ and $\vec{r}_3$ using scalar constants $c_1$ and $c_3$. Similarly, we expressed the other two position vectors, $\vec{r}_1$ and $\vec{r}_3$, in terms of $\vec{r}$ and $\dot{\vec{r}}$ using time-dependent scalar functions $f_1$, $f_3$, $g_1$, $g_3$.

Substituting these expressions into the equations, we obtained relationships such as Formula 3

$$\vec{r}_2 = c_1\vec{r}_1 + c_3\vec{r}_3 \tag{3}$$

Using conservation of momentum we define scalar constants $c_1$ and $c_3$ in terms of scalar functions $f_1$, $f_3$, $g_1$, $g_3$.

We rearranged the equations to show that $c_1r_1 + c_2r_2 + c_3r_3 = 0$, where $c_2 = -1$ and expressed this as scalar equations of range involving known directions $\hat{\rho}$ and Sun vectors $\vec{R}$.

$$\begin{aligned}
\rho_1 &= \frac{c_1D_{11} + c_2D_{12} + c_3D_{13}}{c_1D_0} \\
\rho_2 &= \frac{c_1D_{21} + c_2D_{22} + c_3D_{23}}{c_2D_0} \\
\rho_3 &= \frac{c_1D_{31} + c_2D_{32} + c_3D_{33}}{c_3D_0}
\end{aligned} \tag{4}$$

The scalar equations of the range provided formulas for each range value,where the $D_{ij}$ are constants described by the following set of vector equations 5.

$$\begin{aligned}
D_0 &= \hat{\rho}_1 \cdot (\hat{\rho}_2 \times \hat{p}_3) \\
D_{1j} &= (\vec{R}_j \times \hat{\rho}_2) \cdot \hat{\rho}_3 \\
D_{2j} &= (\hat{\rho}_1 \times \vec{R}_j) \cdot \hat{\rho}_3 \\
D_{3j} &= \hat{\rho}_1 \cdot (\hat{\rho}_2 \times \vec{R}_j)
\end{aligned} \tag{5}$$

Notably, the critical $D_0$ term influenced the success of the Method of Gauss. If the observations show little curvature or great circle motion, $D_0$ approaches zero, leading to divergent solutions.

To determine the vectors $\vec{r}$ and $\dot{\vec{r}}$, we faced a circular dependency as $f$ and $g$ functions depended on the orbital elements, which in turn relied on $\vec{r}$ and $\dot{\vec{r}}$. To address this, we employed an iterative process. Starting with an initial guess or value, we countiously iterated to improve our values $\vec{r}$ and $\dot{\vec{r}}$ until convergence. For the first iteration, we used a truncated Taylor series expansion for $f$ and $g$, considering only the first terms.

The determination of $r_2$, required for the initial iteration, posed a challenge as relying on guesses or predicted values would introduce bias. Therefore, we mathematically determined $r_2$ using the Scalar Equation of Lagrange.

### *4.1.2. Scalar Equation of Lagrange*

The scalar equation of Lagrange is an eighth-order polynomial equation whose real, positive roots approximate the possible r2 values [10]. Each value must be tested through the entire Method of Gauss. As it is an approximation, some and possibly all roots may not converge to the correct solution. The formula of the Scalar Equation of Lagrange:

$$r_2^8 + ar_2^6 + br_2^3 + c = 0 \tag{6}$$

where $a$, $b$, and $c$ are constants described by the equations 7

$$\begin{aligned} a &= -(A^2 + AE + F) \\ b &= -\mu(2AB + BE) \\ c &= -\mu^2 B^2 \end{aligned} \tag{7}$$

We can express A, B, E, and F components of the above equation using Formula 8 where $A_1, A_3, B_1$, and $B_3$ components are themselves described by the following set of equations 9 and D components are obtained using the Method of Gauss.

$$\begin{aligned} A &= \frac{A_1 D_{21} - D_{22} + A_3 D_{23}}{-D_0} \\ B &= \frac{B_1 D_{21} + B_3 D_{23}}{-D_0} \\ E &= -2(\hat{\rho}_2 \cdot \vec{R}_2) \\ F &= R_2^2 \end{aligned} \tag{8}$$

The positive roots of the Lagrange equation are then used in the first iteration of $f$ and $g$ functions as mentioned above, and then the method is iterated, but after the first iteration, more accurate $f$ and $g$ functions can be used.,

$$\begin{aligned} A_1 &= \frac{\tau_3}{\tau} \\ A_3 &= -\frac{\tau_1}{\tau} \\ B_1 &= A_1^6 \cdot (\tau^2 - \tau_3^2) \\ B_3 &= A_3^6 \cdot (\tau^2 - \tau_1^2) \end{aligned} \tag{9}$$

## 5. Results

### *5.1. Monte Carlo Simulations*

In a Monte Carlo simulation, input values are randomly varied following a weighted distribution that corresponds to a Gaussian normal distribution. For each input variable, the normal distribution is centered around the input value, with one standard deviation equal to the input uncertainty [13]. These slightly varied values are utilized as inputs in the Method of Gauss, and subsequently, slightly adjusted orbital elements are obtained. As the number of iterations for the Monte Carlo simulation increases, the outputs should approximate a normal curve in their placement. This is represented by several histograms in figure 2.

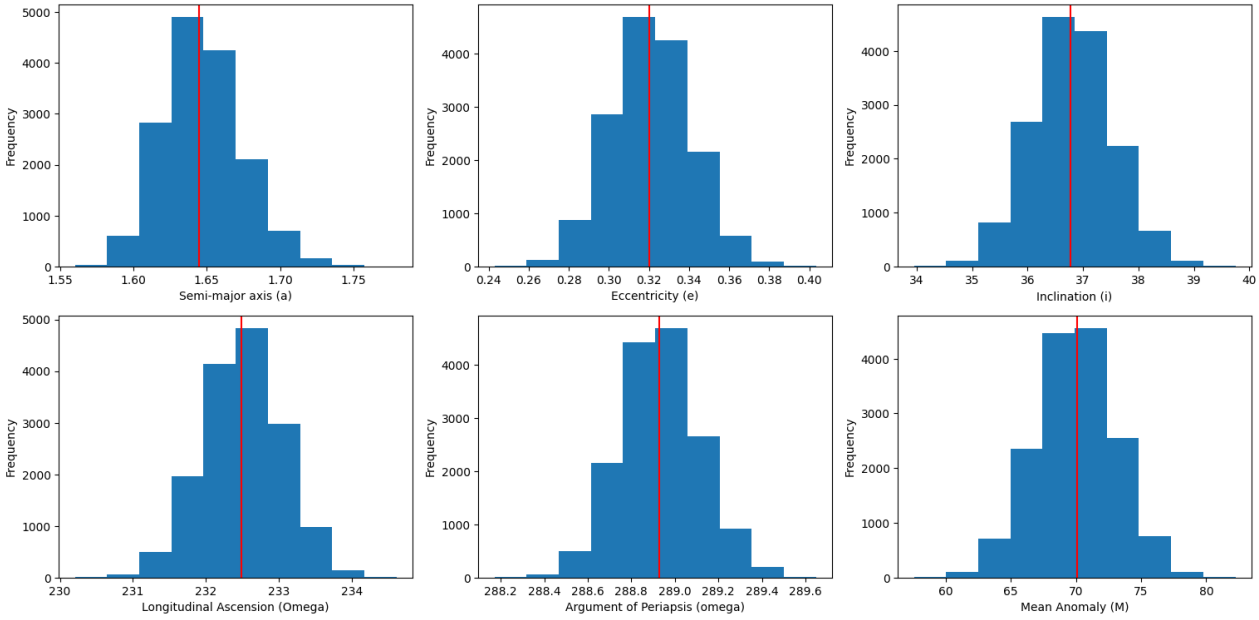


Figure 2: Histogram obtained through Monte Carlo simulations detailing the distribution of the calculated orbital elements, where the red vertical lines refer to the expected value for its respective orbital element.

### *5.2. The Orbital Elements*

After setting up the code taking into consideration the methods referenced in Section 4.1, we were able to obtain the orbital elements (Table 4). These elements were calculated using a Monte Carlo simulation [5] with $5^6$ iterations and assuming a worst-case scenario uncertainty of 0.5". This was mainly done because there were multiple factors that had the possibility of affecting the accuracy of our data, such as the especially low apparent magnitude of 3553 Mera. Afterward, we get each object's SDOM (Standard Deviation of the Mean), as well as the percentage of difference in comparison to the data presented by the JPL Horizons' Web Application. The calculated data was also included within Figure 2 for a better representation of the distribution.

| Orbital Elements | Calculated Value | SDOM | Difference (%) |
|---|---|---|---|
| **Semi-major axis (a)** | 1.65 AU | 0.0266 | 0.1538 |
| **Eccentricity (e)** | 0.32 | 0.0199 | 0.2200 |
| **Inclination (i)** | 36.8 ° | 0.7205 | 0.0075 |
| **Longitudinal Ascension ($\Omega$)** | 232.5 ° | 0.5406 | 0.0031 |
| **Argument of Periapsis ($\omega$)** | 288.9 ° | 0.1819 | 0.0010 |
| **Mean Anomaly (M)** | 70 ° | 3.0629 | 0.0302 |

Table 4: Calculated orbital elements along with their percentage of error and SDOM using a Monte Carlo simulation.

## 6. Discussion

Our results turned out to be very similar to those presented by the JPL Horizon's Web Application, with the greatest variations being just a couple tenths of a percentage point off. Additionally, we were able to accurately recover the RA (Table 5) and declination (Table 6) of our observations after re-inputting the position and velocity vectors that we got after iterating through the orbit determination code.

We believe that even though our results seem to be very accurate and barely differ from those presented by JPL, there were still a lot of factors that could have affected the quality of the said results. For starters, the climatological conditions during most of our observations were not particularly favorable. For the majority of our observations, we struggled with cloudy weather, which made it especially difficult for us to spot the asteroid within our images, as well as determine an accurate centroid for it. In addition to that, the asteroid's magnitude was barely within our telescope's visibility range and only got dimmer as time went by, further obstructing the progress of our research.

For conducting an improved study, we would recommend choosing a moment in time when Mera 3553 had a lower apparent magnitude, as that would greatly facilitate its analysis. Additionally, we would recommend finding a place with better climatological conditions, as Chapel Hill is prone to rainy weather which precludes any observations.

| RA | Calculated | Expected | Difference (%) |
|---|---|---|---|
| **First Observation** | 16:07:27.66 | 16:07:27.90 | 2.81E-4 |
| **Second Observation** | 15:58:25.00 | 15:58:25.01 | 1.01E-5 |
| **Third Observation** | 15:58:19.53 | 15:58:19.51 | 2.54E-5 |

Table 5: Comparison of the calculated and expected Right Ascension for our three observations (in hh:mm:ss), along with their respective percentage errors.

## 7. Conclusion

This paper has demonstrated how to calculate the orbit of a near-Earth asteroid while only needing three observations. Through advanced approaches such as the Scalar Equations of La-

| Declination | Calculated | Expected | Difference (%) |
|---|---|---|---|
| **First Observation** | 19°20’ 44.25” | 19°20’ 45.39” | 8.81E-5 |
| **Second Observation** | 21°20’ 20.37” | 21°20’ 20.39” | 1.26E-6 |
| **Third Observation** | 21°19’ 17.00” | 21°19’ 16.82” | 1.36E-5 |

Table 6: Comparison of the calculated and expected declinations for our three observations (in degrees, minutes, seconds), along with their respective percentage errors.

grange and the Method of Gauss, we were able to, not only generate the asteroid’s position and velocity vectors, but also use them to calculate its orbital elements and even recreate its RA and declination to within fractions of an arcsecond.

Although we are satisfied with our results, if the reader would like to build upon this study, we would recommend implementing a code that is able to take into consideration more than three observations by using partial derivatives and a Least Squares method similar to that referenced in Section 2.2. This would greatly improve the accuracy of our current measurements, as it would be very similar to fitting a non-linear line that could better match our points. Additionally, we believe it would be very insightful to calculate a long-term orbit for the asteroid, showing the different possibilities of its position many years into the future, also taking into consideration the effects of other planets within its orbit, so that we can determine if there is any potential threat of crashing into our planet or some other object within our solar system. Finally, we believe it would be really interesting to calculate 1985 JA’s spin and how that is related to fluctuations within its apparent magnitude.

## 8. Appendix

### *8.1. Submission data for the MPC*

The following figure depicts the observational data of 1985 JA that was sent to the International Astronomical Union’s Minor Planet Center to be published.

```
03553         C2023 06 17.26550 16 07 27.89 +19 20 45.39          17.1 R      TBD
03553         C2023 06 17.27015 16 07 27.63 +19 20 49.37          17.1 R      TBD
03553         C2023 06 17.27565 16 07 27.41 +19 20 52.01          17.6 R      TBD

03553         C2023 07 05.18288 15 58 25.19 +21 20 20.23          18.8 R      TBD
03553         C2023 07 05.19421 15 58 25.12 +21 20 20.44          18.7 R      TBD
03553         C2023 07 05.20125 15 58 25.01 +21 20 20.81          18.5 R      TBD

03553         C2023 07 08.28422 15 58 19.49 +21 19 16.85          18.5 R      U69
03553         C2023 07 08 28662 15 58 19.50 +21 19 16.82          18.7 R      U69
03553         C2023 07 08 28902 15 58 19.51 +21 19 16.82          18.6 R      U69
```

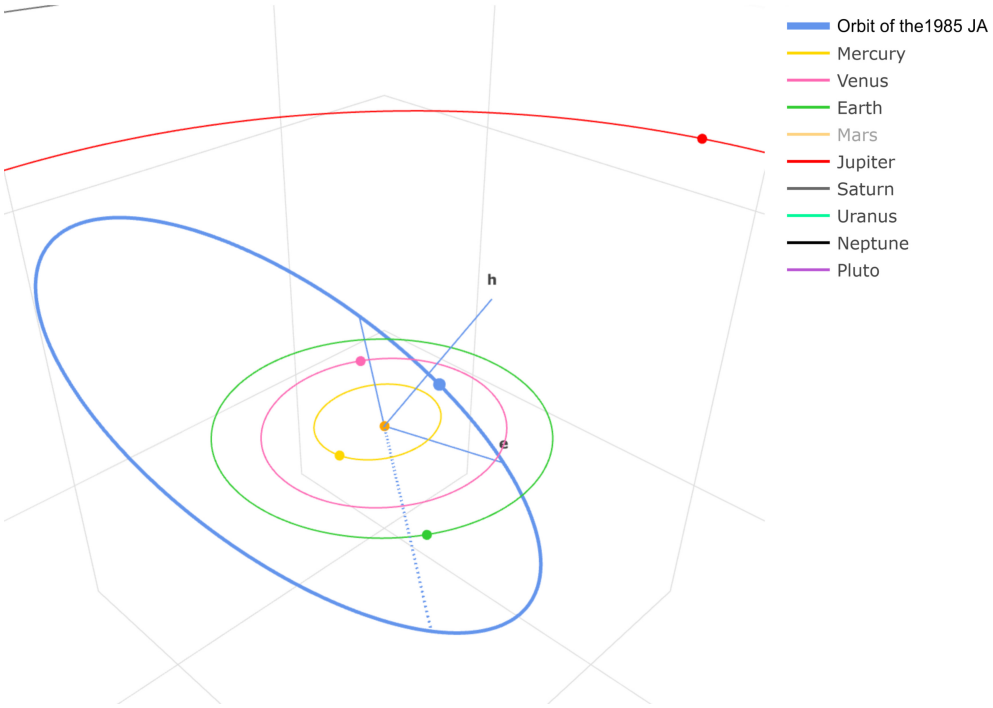


Figure 3: Orbit of the 1985 JA asteroid

### *8.2. Orbit visualization*

We also visualized the orbit of our asteroid using calculated orbital elements and position vectors. These visualizations, shown in Figure 3, provided a graphical representation of the asteroid's trajectory, allowing us to observe its motion more intuitively. The visualization served as a useful tool for better understanding the orbital behavior and dynamics of the asteroid. It provided a visual representation that aided in the interpretation and analysis of the asteroid's orbit, contributing to a deeper understanding of its motion about the Sun and the Earth.

## Acknowledgements

We would like to express our special gratitude to Dr. Michael Hannawald and Dr. Jesse Feddersen for their valuable lectures on mechanics, relativity, quantum mechanics, astrometry, and photometry, and other fascinating aspects of astrophysics. Special thanks to our site director Dr. Nicole Ice for prioritizing our safety during the program, and Dr. Aaron Bauer for his exceptional guidance in teaching us the fundamentals of programming and providing us with engaging programming problem sets. We are also very grateful to our wonderful TAs - Ian Kimbell, Julio Morales, Lucy Williamson, and Feli Xiao- for their mentorship, encouragement, and assistance during our working sessions. Additionally, we also acknowledge the University of North Carolina Chapel Hill for hosting our program and the Morehead Observatory for granting us access to their facilities. Finally, we would like to express our sincere gratitude to the Summer Science Program for providing us with this incredible opportunity to delve into the world of scientific research.

## References


[1] 2022, DART

[2] Agency, T. E. S. 2022, 30 000 near-Earth asteroids discovered and rising

[3] Davis, P., & Carnet, S. 2023, Comets

[4] for Outer Space, U. N. O. 2023, Near-Earth Objects

[5] Harrison, R. L. 2010in , American Institute of Physics, 17–21

[6] Jet Propulsion Laboratory. [2023], Horizons Web Application, [Online]. Available: https://ssd.jpl.nasa.gov/horizons/app.html/, jPL's Solar System Dynamics (SSD) group

[7] Kennedy, M. 2022, Help us protect our home from asteroids

[8] Milani, A., & Gronchi, G. 2010, Theory of orbit determination (Cambridge University Press)

[9] Mou, J., & Webster, I. 2023, Mars-crossing Asteroids | Space Reference

[10] Moyer, T. D. 1971, Mathematical formulation of the double precision orbit determination program/dpodp, Tech. rep.

[11] NASA. 2021, What is an Asteroid?

[12] of Oregon, U. 2011, Solar System Debris

[13] Raychaudhuri, S. 2008, in 2008 Winter simulation conference, IEEE, 91–100

[14] Rieke, G. n/a, Solar System Debris

[15] White, J. 2021, Debris Disks: What Can We Learn from the Leftovers of the Planet Formation Process?